Electrocatalysis | *Hot Paper*

Electrocatalytic Proton Reduction by a Cobalt Complex Containing a Proton-Responsive Bis(alkylimdazole)methane Ligand: Involvement of a C–H Bond in H_2 Formation

Pradip Ghosh,[a, d] Sander de Vos,[a] Martin Lutz,[b] Frederic Gloaguen,[c] Philippe Schollhammer,[c] Marc-Etienne Moret,[a] and Robertus J. M. Klein Gebbink*[a]

Abstract: Homogeneous electrocatalytic proton reduction is reported using cobalt complex [**1**]$(BF_4)_2$. This complex comprises two bis(1-methyl-4,5-diphenyl-1*H*-imidazol-2-yl)methane ($HBMIM^{Ph_2}$) ligands that contain an acidic methylene moiety in their backbone. Upon reduction of [**1**]$(BF_4)_2$ by either electrochemical or chemical means, one of its $HBMIM^{Ph_2}$ ligands undergoes deprotonation under the formation of dihydrogen. Addition of a mild proton source (acetic acid) to deprotonated complex [**2**](BF_4) regenerates protonated complex [**1**]$(BF_4)_2$. In presence of acetic acid in acetonitrile solvent [**1**]$(BF_4)_2$ shows electrocatalytic proton reduction with a k_{obs} of $\approx 200\ s^{-1}$ at an overpotential of 590 mV. Mechanistic investigations supported by DFT (BP86) suggest that dihydrogen formation takes place in an intramolecular fashion through the participation of a methylene C–H bond of the $HBMIM^{Ph_2}$ ligand and a Co^{II}–H bond through formal heterolytic splitting of the latter. These findings are of interest to the development of responsive ligands for molecular (base)metal (electro)catalysis.

Introduction

The generation of dihydrogen (H_2) from protons has been extensively investigated in recent times in view of the prospective use of H_2 as a carbon-free energy carrier.[1,2] Several classes of molecular electrocatalysts have been designed to facilitate the reduction of protons to hydrogen (hydrogen evolution reaction, HER) and efforts have been sustained to develop more efficient catalysts.[3–18] The use of first row, earth-abundant transition-metal ions in combination with a suitable cooperative/proton- or electron-responsive ligand has found particular interest in the development of homogeneous catalysts for HER reactions.[19,20] Dubois and Bullock et al. have developed Ni-catalysts $[Ni(P^R_2N^{R'}_2)_2]^{2+}$ (Figure 1a), in which the catalytic activity is facilitated by the incorporation of a pendant amine functionality that relays protons during catalysis.[8–10] The positioning of pendant N–H protons in the ligand tunes the efficiency of these catalysts. Eisenberg and Holland reported the use of the

[a] Dr. P. Ghosh, S. de Vos, Dr. M.-E. Moret, Prof. Dr. R. J. M. Klein Gebbink
Organic Chemistry and Catalysis
Debye Institute for Nanomaterials Science, Utrecht University
Universiteitsweg 99, 3584 CG, Utrecht (The Netherlands)
E-mail: r.j.m.kleingebbink@uu.nl

[b] Dr. M. Lutz
Crystal and Structural Chemistry
Bijvoet Centre for Biomolecular Research
Utrecht University, Padualaan 8, 3584 CH, Utrecht(The Netherlands)

[c] Dr. F. Gloaguen, Prof. Dr. P. Schollhammer
UMR 6521, CNRS, Université de Bretagne Occidentale
CS 93837, 29238 Brest (France)

[d] Dr. P. Ghosh
Present address: Department of Chemistry, University of Hamburg
Martin-Luther-King-Platz 6, 20146 Hamburg (Germany)

Supporting information and the ORCID identification number(s) for the author(s) of this article can be found under:
https://doi.org/10.1002/chem.201905746.

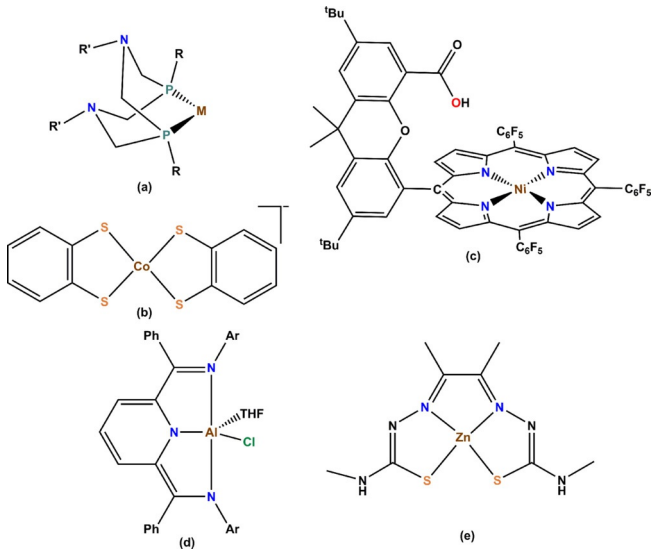

Figure 1. Examples of molecular HER catalysts.

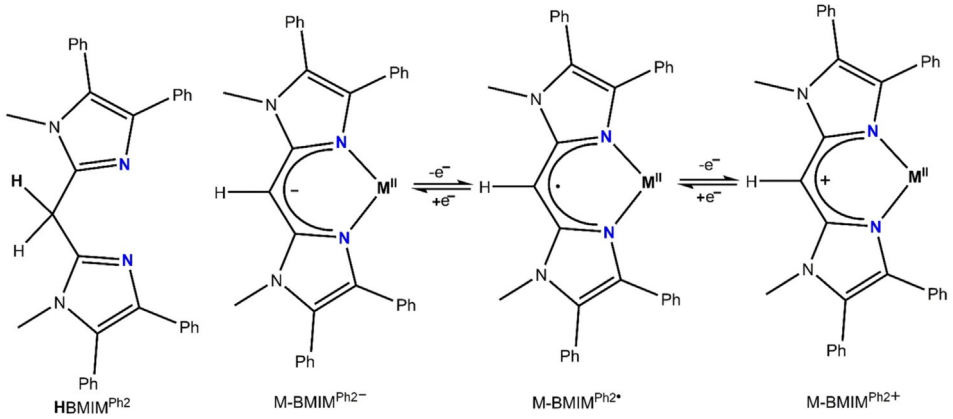

Scheme 1. The HBMIM^{Ph_2} ligand (left) and ligand-centered redox events in [M(BMIM$^{Ph_2-}$)$_2$] complexes (right).

dithiolatecobalt complex $[Co(bdt)_2]^-$ (bdt = 1,2-benzenedithiolate; Figure 1b) as photocatalyst and electrocatalyst for HER.[11,12] Later, mechanistic aspects of proton reduction by substituted dithiolene cobalt complexes have been reported.[21–23] The high activity of the $[Co(bdt)_2]^-$ catalyst was rationalized by the use of a redox-active dithiolate ligand that can store/release electrons and participation of the sulfur donors in proton relay during catalysis.

The development of efficient catalysts for HER relies on the understanding of the fundamental steps involved in catalysis. A commonly proposed mechanism is the formation of an intermediate metal hydride (M–H) species that undergoes reduction, followed by protonation resulting in dihydrogen evolution.[20,24,25] In addition, examples of ligand-mediated HER have been reported that do not rely on the formation of M–H intermediates. Nocera and co-workers have reported nickel "hangman" porphyrin complexes (Figure 1c), in which the conjugated porphyrin system dearomatizes upon reduction.[26] The *meso*-carbon atom in the dearomatized system accepts a proton from either the hanging carboxylic acid group or from an external proton source to produce a phlorin intermediate which is the active species that stores electrons in the C–H bond. In this example, proton-coupled electron-transfer processes (PCET)[27–29] play a critical role to avoid high-energy intermediates in the catalytic cycle. Berben et al. have reported on an aluminium-based HER catalyst derived from a phenyl-substituted bis(imino)pyridine ligand in which both proton- and electron transfer are mediated by the ligand backbone, that is, without involvement of the Al center (Figure 1d).[16] Grapperhaus et al. have synthesized a redox-active thiosemicarbazone ligand where the free ligand and its zinc complex (Figure 1e) are used as electrocatalysts for proton reduction.[18]

Recently, we have reported on the synthesis of the diimine ligand bis(1-methyl-4,5-diphenyl-1*H*-imidazol-2-yl)methane (HBMIM^{Ph_2}) in which the ligand framework is very similar to well-known β-diketimine, or HNacNac, ligand systems (Scheme 1).[30] The coordination and ligand-based oxidation chemistry of the corresponding anionic ligand, BMIM$^{Ph_2-}$, has been studied for its cobalt and zinc complexes, [M(BMIM$^{Ph_2-}$)$_2$] (M = Co and Zn). Through cyclic voltammetric analysis, it was observed that these complexes undergo a total of four single-electron oxidation events that are all ligand based. The first two oxidations are at negative potentials vs. the ferrocene/ferrocinium couple, which has enabled us to isolate and characterize the singly and doubly oxidized complexes, overall covering three different oxidation states.[30]

In this paper, we report the synthesis of cobalt complex [Co(HBMIM^{Ph_2})$_2$](BF$_4$)$_2$, [**1**](BF$_4$)$_2$, based on the neutral diimine ligand HBMIM^{Ph_2}, which is found to be an electrocatalyst for the HER reaction. Our combined experimental and DFT studies support that [**1**](BF$_4$)$_2$ undergoes H-atom loss upon reduction (chemically or electrochemically) resulting in formal deprotonation and generates cobalt complex [Co(HBMIM^{Ph_2})(BMIM$^{Ph_2-}$)](BF$_4$), [**2**](BF$_4$) containing one deprotonated BMIM$^{Ph_2-}$ligand. Protonation of the coordinated BMIM$^{Ph_2-}$ ligand restores the original complex [**1**](BF$_4$)$_2$ and closes a catalytic cycle. Isolation and characterization of [**2**](BF$_4$) in combination with mechanistic investigations using DFT suggest that a ligand C–H moiety and an intermediate Co–H moiety are involved in the dihydrogen formation step, providing a unique HER mechanism.

Results and Discussion

Synthesis and characterization: X-ray, electrochemistry and electronic structure analysis

Cobalt complex [**1**](BF$_4$)$_2$ was synthesized by reacting Co(BF$_4$)$_2$·6H$_2$O and bis(1-methyl-4,5-diphenyl-1*H*-imidazol-2-yl)-methane (HBMIM^{Ph_2}) in a 1:2 molar ratio in THF. The pink complex of composition [Co(HBMIM^{Ph_2})$_2$](BF$_4$)$_2$ was isolated from the reaction mixture in quantitative yield by precipitation (Scheme 2).

ESI-MS analysis of this complex in acetonitrile shows intense peaks at 509.6853 amu and 1106.3882 amu for $[\mathbf{1}]^{2+}$ (calcd: 509.6980 amu) and $\{[\mathbf{1}](BF_4)\}^+$ (calcd: 1106.4000 amu), respectively (Figure S1). The ^{1}H NMR spectrum of [**1**](BF$_4$)$_2$ in CD$_3$CN shows broad signals between −30 and 200 ppm, clearly indicating its paramagnetic nature (Figure S2). Solution state magnetic susceptibility measurement by Evans method confirmed

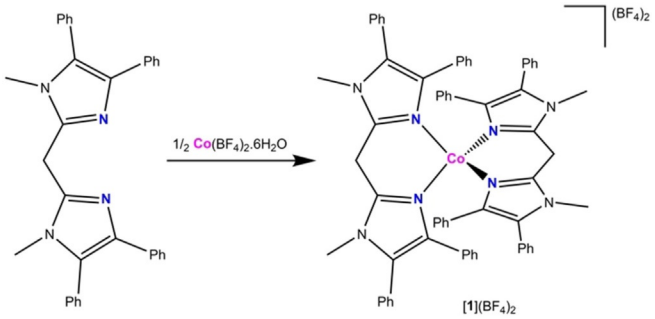

Scheme 2. Synthesis of $[\mathbf{1}](BF_4)_2$.

that $[\mathbf{1}](BF_4)_2$ is a high spin cobalt(II) complex ($\mu_{eff} = 3.82\ \mu_B$). The complex has been characterized using single-crystal X-ray structure determination. The molecular structure of $[\mathbf{1}](BF_4)_2$ is shown in Figure 2, while key bond distances and angles are compiled in Table S1. The asymmetric unit of $[\mathbf{1}](BF_4)_2$ contains two independent molecules and the structure reveals a twisted tetrahedral geometry of the complex with a twist angle in between the two nearly planar NCCCN chelators (N1-C2-C1-C18-N3) of 65.68–71.23°.

The redox behavior of $[\mathbf{1}](BF_4)_2$ was examined by CV in CH_3CN using $[Bu_4N]PF_6$ as supporting electrolyte. $[\mathbf{1}](BF_4)_2$ displays two reduction peaks at −1.96 V (R1) and −2.36 V (R2) vs. Fc/Fc^+ (Fc = ferrocene), while in the reverse scan (cathodic to anodic) an oxidation peak (O1) was noted at −0.64 V (Figure 3a). The segmented cyclic voltammogram (black line) indicates that the first chemically irreversible reduction is responsible for the appearance of the oxidation; this CV response is consistent with an electrochemical step followed by a chemical reaction (EC mechanism, vide infra).[27–29] Consecutive cathodic scans confirm the accumulation in the vicinity of the electrode of a stable product reversibly oxidized at ca. −0.7 V (see Figure S3). To gain insight in the second reduction process R2, CVs were recorded at increasing scan rates (v) (Figure S4). The peak current function $i_{p,R2}/v^{1/2}$ and the peak current ratio $i_{p,R2}/i_{p,R1}$ are both independent of v (Figure S4, inset). It is therefore difficult to conclude whether or not R2 is related to R1 based on this CV analysis (vide infra). A spectroelectrochemistry experiment in $CH_3CN/[Bu_4N]PF_6$ was performed to examine the optical changes associated with the primary reduction of $[\mathbf{1}](BF_4)_2$ using an optically transparent thin layer electrochemical (OTTLE) cell. $[\mathbf{1}](BF_4)_2$ shows weak d–d transitions at 555 and 510 nm, while the electro-generated, reduced complex absorbs strongly at 370 nm (Figure 3b). The $HBMIM^{Ph_2}$ ligand itself is not reduced in the potential range up to −2.6 V vs. Fc/Fc^+ in $CH_2Cl_2/[Bu_4N]PF_6$ (Figure S5).

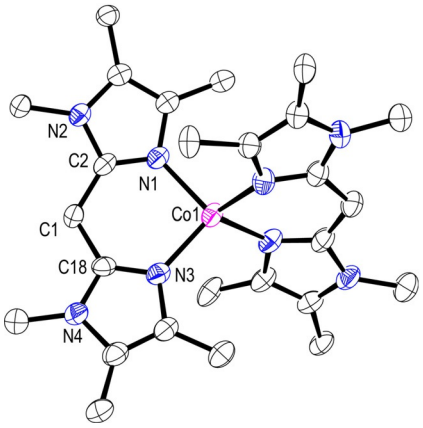

Figure 2. Displacement ellipsoid plot of $[\mathbf{1}]^{2+}$ (50% probability). Phenyl rings, methyl H-atoms, BF_4 counter anions, and disordered solvent molecules have been omitted for clarity. Only one of two independent molecules is shown.

Next, we treated $[\mathbf{1}](BF_4)_2$ with one equivalent of KC_8 in THF, which resulted in the isolation of brown complex $[\mathbf{2}](BF_4)$ in 72% yield (Scheme 3). Immediate effervescence was observed upon the addition of KC_8 to the solution of $[\mathbf{1}](BF_4)_2$ which indicates the formation of a gaseous by-product. The UV-vis spectrum of isolated $[\mathbf{2}](BF_4)$ in THF is identical to that of the complex generated in the spectroelectrochemical experiment, *viz.* the chemically reduced complex is in accordance with the electrochemically reduced complex (Figure S6). $[\mathbf{2}](BF_4)$ is paramagnetic as shown by its ^1H NMR spectrum (Figure S7). The solution state magnetic moment measurement by Evans method indicates the presence of three unpaired spins ($\mu_{eff} = 3.7\ \mu_B$). Hence, no change in the overall spin state has taken place upon reduction of $[\mathbf{1}](BF_4)_2$. The ESI-MS spectrum of $[\mathbf{2}](BF_4)$ in THF shows an intense peak at m/z 1018.3724 amu, which matches with the chemical composition of $[Co(BMIM^{Ph_2-})(HBMIM^{Ph_2})]^+$, that is, a Co^{II} center coordinated by one anionic ligand and one neutral ligand. The simulated isotope pattern for this composition (m/z 1018.3882 amu) matches well with the experimental spectrum (Figure S8).

We have obtained suitable crystals of compound $[\mathbf{2}]BF_4$ for single-crystal X-ray diffraction. Analysis of the diffraction data resulted in a structure that cannot be distinguished from the structure of $[Co(BMIM^{Ph_2-})(BMIM^{Ph_2\bullet})](BF_4)$ that we described earlier.[30] Brown $[\mathbf{2}]BF_4$ and green $[Co(BMIM^{Ph_2-})(BMIM^{Ph_2\bullet})](BF_4)$ have distinctly different physical properties and have been synthesized in different ways. Yet, their structural difference (a single hydrogen atom) cannot be ascertained through X-ray analysis.

Overall, we conclude that formal deprotonation of one of the $HBMIM^{Ph_2}$ ligands takes place upon reduction of $[\mathbf{1}](BF_4)_2$ via either chemical or electrochemical means. Initial reduction is likely to reduce the Co^{II} center in $[\mathbf{1}](BF_4)_2$ to generate a Co^{I} intermediate. Subsequent electron-transfer from the reduced metal center to one of the coordinated $HBMIM^{Ph_2}$ ligands is envisioned to occur concomitantly with cleavage of a methylene C–H bond and formation of hydrogen gas, resulting in a Co^{II} complex containing one neutral and one anionic ligand.

The CV of complex $[\mathbf{2}](BF_4)$ shows two reversible oxidation peaks at −0.66 V and 0.35 V, along with one irreversible reduction peak at −2.39 V (Figure 4). The small reduction peak observed at −1.97 V originates from $[\mathbf{1}]^{2+}$, formed via protonation of $[\mathbf{2}]^+$ by the solvent (CH_3CN or residual H_2O). The oxidative responses at −0.66 V and 0.35 V are due to oxidation of the anionic ligand and generate π-radical and cationic forms of the ligand, respectively.[30,31] The reduction at −2.39 V is ascribed

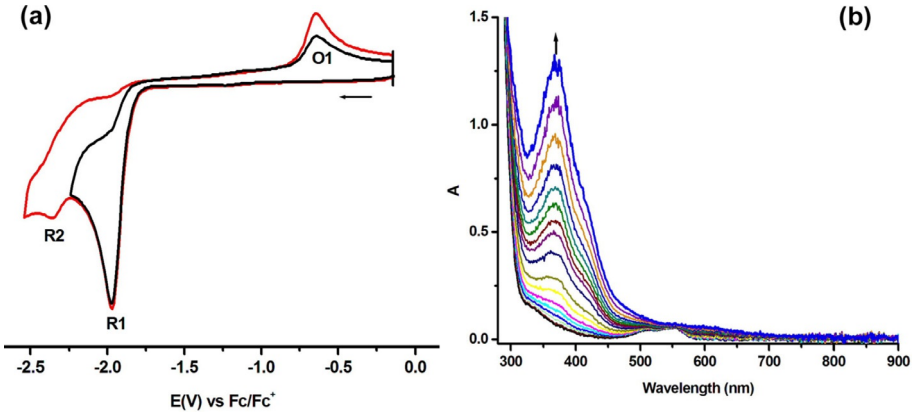

Figure 3. (a) CV of complex $[\mathbf{1}]^{2+}$ in $CH_3CN/[Bu_4N]PF_6$ (scan rate 100 mV s^{-1}) (b) UV-vis spectral change upon reduction of $[\mathbf{1}]^{2+}$ in $CH_3CN/[Bu_4N]PF_6$.

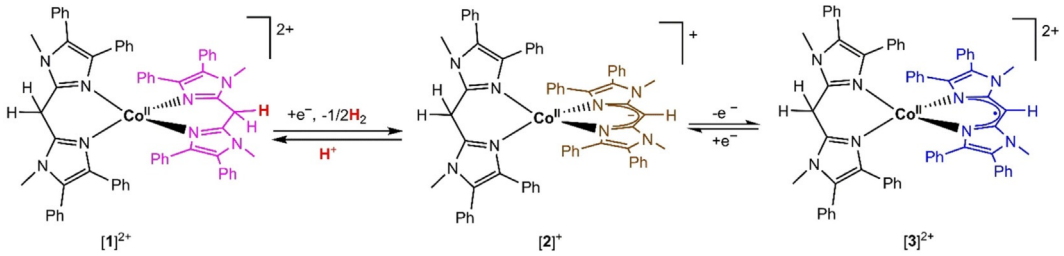

Scheme 3. Chemical changes associated with redox events operative in the coordinated $HBMIM^{Ph_2}$ ligand. The color of the participating ligand represents the color of the isolated cobalt complex.

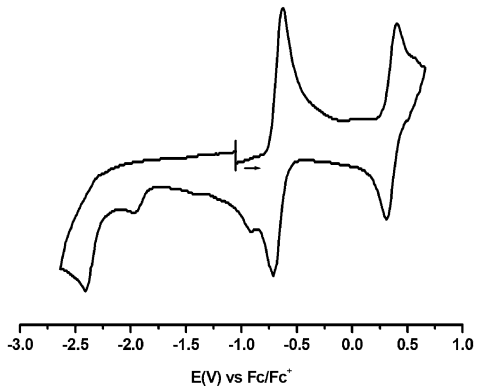

Figure 4. CV of $[\mathbf{2}](BF_4)$ in $CH_3CN/[Bu_4N]PF_6$ (scan rate 100 mV s^{-1}).

to a Co(II/I) couple. A comparison of the peak positions on the CV responses (reductive as well oxidative) shown in Figures 3 and 4 confirm that the primary reduction of $[\mathbf{1}]^{2+}$ gives $[\mathbf{2}]^{+}$ through an EC mechanism. For a clean ECE mechanism, R1 and R2 should have approximately the same peak heights. The unequal peak heights of R1 and R2 in the CV of $[\mathbf{1}](BF_4)_2$ are likely caused by the occurrence of a parallel chemical step that also consumes the reduced intermediate $[\mathbf{1}]^{+}$.

We succeeded to oxidize complex $[\mathbf{2}](BF_4)$ using one equivalent of ferrocinium tetrafluoroborate ($FcBF_4$) on a synthetic scale and deep blue $[\mathbf{3}](BF_4)_2$ was isolated. The isolated complex $[\mathbf{3}](BF_4)_2$ is also paramagnetic, as supported by its ^{1}H NMR spectrum (Figure S9). The solution-state magnetic measurement by Evans method indicates the presence of two-unpaired electrons ($\mu_{eff} = 2.9\ \mu_B$). $[\mathbf{3}](BF_4)_2$ was also characterized by single-crystal X-ray structure determination, which shows that it has a distorted tetrahedral geometry with a twist angle between the two NCCCN chelators (N1-C2-C1-C18-N3) of 70.1(4)° (Figure S10).

The electronic structures of the three isolated cobalt complexes $[\mathbf{1}]^{2+}$, $[\mathbf{2}]^{+}$ and $[\mathbf{3}]^{2+}$ were examined by DFT calculations at the BP86 level as implemented in Gaussian 09.[32] The most stable states for $[\mathbf{1}]^{2+}$ and $[\mathbf{2}]^{+}$ are spin quartets, in accordance with the solution state magnetic data. Mulliken spin densities of 2.59 and 2.51 on the Co centers in $[\mathbf{1}]^{2+}$ and $[\mathbf{2}]^{+}$, respectively, support a high-spin Co^{II} configuration in both cases. The experimental solution magnetic moment for $[\mathbf{3}]^{2+}$ indicates an $S = 1$ ground state, which would be consistent with either of the following two formulations: *i*) an intermediate spin Co^{III} ($S_{Co} = 1$) with one anionic ligand ($S_{BMIMPh_2^-} = 0$) and one neutral ligand ($S_{HBMIMPh_2} = 0$), or *ii*) a high-spin Co^{II} ($S_{Co} = 3/2$) with one neutral ligand ($S_{HBMIMPh_2} = 0$) and one ligand π-radical ($S_{BMIMPh_2^\bullet} = 1/2$) that is antiferromagnetically coupled with the Co center. DFT calculations for $[\mathbf{3}]^{2+}$ favor the latter description. The broken symmetry BS(3,1) and spin unrestricted ($S = 1$) calculations for $[\mathbf{3}]^{2+}$ yield an identical solution, in which the $S = 1$ ground state is attained by antiferromagnetic coupling of the single unpaired electron on the ligand with one of the three unpaired spins in one of the t_2 orbitals of the tetrahedral Co^{II} center (Figure 5). Accordingly, Mulliken analysis of the spin

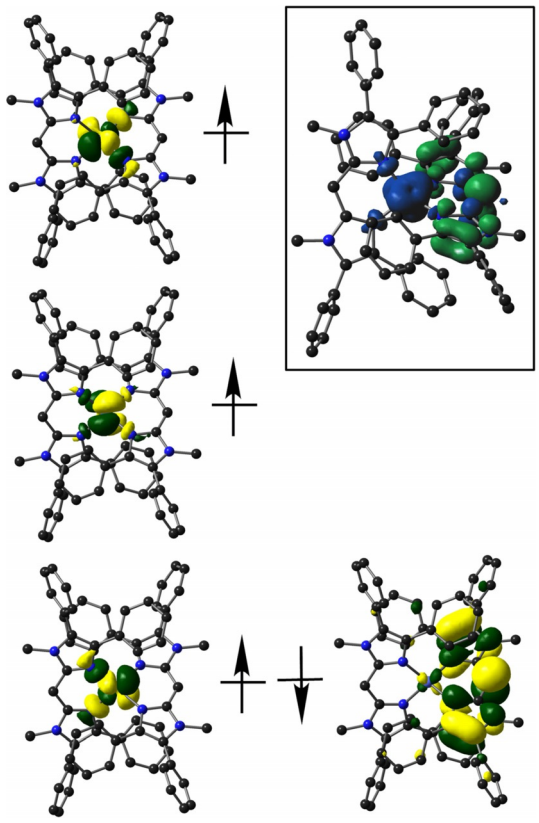

Figure 5. Qualitative MO diagram for complex $[\mathbf{3}]^{2+}$ derived from BS(3,1) calculations (Inset: spin density plot). Active molecular orbitals are shown; the full diagram is provided in the Supporting Information (Figure S11).

density yields an α-spin density of ≈2.49 electron spin at the Co^{II} center and a net β-spin density of ≈−0.48 on the $BMIM^{Ph_2\bullet}$ ligand (Figure 5, inset). Accordingly, the electronic structure of complex $[\mathbf{3}]^{2+}$ is best described as $[Co^{II}(HBMIM^{Ph_2})(BMIM^{Ph_2\bullet})]^{2+}$.

Characterization of complex $[\mathbf{3}](BF_4)_2$ by various spectroscopic techniques as well as electronic structure analysis clearly indicates that 1-electron oxidation of $[\mathbf{2}](BF_4)$ happens at the deprotonated ligand to produce a neutral π-radical ligand ($BMIM^{Ph_2\cdot}$) in $[\mathbf{3}](BF_4)_2$. The second oxidation at 0.35 V, as indicated by CV (Figure 4), is likely to be ligand-based as well, in line with our earlier analysis of the redox events in Co-complexes featuring two anionic $BMIM^{Ph_2-}$ ligands.[30] The above (electro)chemical transformations converting $[\mathbf{1}](BF_4)_2$ in $[\mathbf{2}](BF_4)$, and subsequently in $[\mathbf{3}](BF_4)_2$ are compiled in Scheme 3.

Our investigations reveal that $[\mathbf{1}](BF_4)_2$ undergoes a formal deprotonation upon (electro)chemical reduction. Additional experiments show that addition of a mild proton source, for example, acetic acid (AcOH), to singly deprotonated complex $[\mathbf{2}](BF_4)$ regenerates the starting, protonated complex $[\mathbf{1}](BF_4)_2$. Addition of CD_3COOD (5 equivalents) to a THF solution of $[\mathbf{2}](BF_4)$ yields a pink-colored complex, in line with the color of $[\mathbf{1}](BF_4)_2$. Subsequent characterization by ESI-MS showed an ion of 510.2099 amu, that is, an ion of mass (m + 1) with respect to the ion $[\mathbf{1}]^{2+}$ indicating the incorporation of a deuterium atom (Figure S12). Hence, the $HBMIM^{Ph_2}$ ligand in $[\mathbf{1}](BF_4)_2$ can act as a proton as well as an electron reservoir (Scheme 3).

This notion is supported by the behavior of Co-complex $[\mathbf{4}](BF_4)_2$ supported by two bis-methylated $Me_2BMIM^{Ph_2}$ ligands, that do not contain a methylene moiety in their backbone (Figure 6, left). Details on the synthesis and characterization of $[\mathbf{4}](BF_4)_2$, including single crystal X-ray structural determination, are provided in the Supporting Information. The CV of $[\mathbf{4}](BF_4)_2$ features an irreversible reduction peak at −1.70 V vs. Fc/Fc^+ in $CH_3CN/[Bu_4N]PF_6$. This potential is ca. 0.26 V more positive than that of the first reduction of $[\mathbf{1}](BF_4)_2$ and is assigned to a $Co^{II/I}$ couple (Figure 3a). The CV of $[\mathbf{4}](BF_4)_2$ does not show the typical second reduction peak observed for $[\mathbf{1}](BF_4)_2$, and shows an oxidation peak in the reverse cathodic to anodic scan at a potential ca. 0.75 V more positive than observed for $[\mathbf{1}](BF_4)_2$. These results corroborate the importance of an acidic methylene unit in the $HBMIM^{Ph_2}$ ligand in the redox chemistry observed for $[\mathbf{1}](BF_4)_2$ (vide infra). Yet, the irreversible nature of the reduction of $[\mathbf{4}](BF_4)_2$ is currently not understood.

Electrocatalytic studies

The reversibility of the (reduction-induced) deprotonation of $[\mathbf{1}](BF_4)_2$ led us to examine this complex as an electrocatalyst for HER. Accordingly, electrocatalytic proton-reduction experiments were carried out in $CH_3CN/[Bu_4N]PF_6$ using acetic acid (AcOH, $pK_a = 22.3$) as a proton source. Upon addition of AcOH to $CH_3CN/[Bu_4N]PF_6$ solutions of $[\mathbf{1}](BF_4)_2$ (0.5 mM), the cathodic current at −1.96 V increases, indicating an electrocatalytic reduction process (Figure 7a). At AcOH concentrations above 80 mM, the current associated with this process is no longer dependent on the acid concentration, but the electrocatalytic

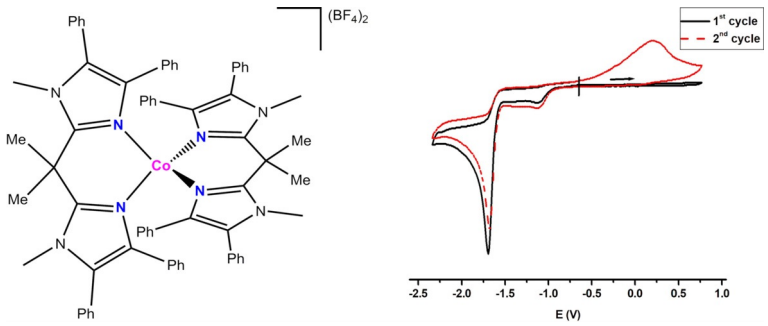

Figure 6. Complex $[\mathbf{4}](BF_4)_2$ (left) and its CV in $CH_3CN/[Bu_4N]PF_6$ (scan rate 100 mV s^{-1}; right).

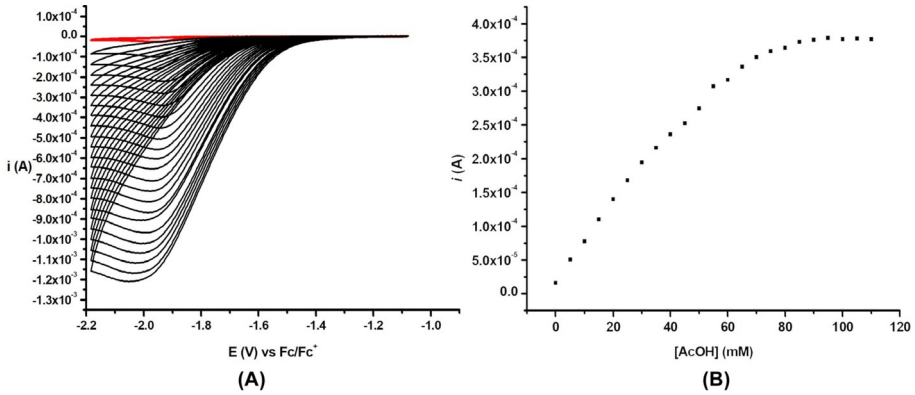

Figure 7. (a) Red line: CV of $[\mathbf{1}](BF_4)_2$ (0.5 mM); black line: addition of 10–240 equivalents of AcOH in $CH_3CN/[Bu_4N]PF_6$ (scan rate = 0.2 V s^{-1}). (b) plot of current (i_{cat}) vs. [AcOH].

wave remains peak shaped indicating a limitation by acid diffusion to the electrode surface (Figure 7b). Under saturating acid conditions, the observed catalytic rate constant gives the upper limit of the turnover frequency, which is $TOF_{max} \approx 200\ s^{-1}$ (Figure S13). The overpotential for hydrogen evolution under these conditions is 590 mV, after considering the homoconjugation effect of AcOH.[33,34] Under non-saturating acid conditions, the catalytic current (i_{cat}) is linearly dependent on acid concentration indicating that the acid is involved in the rate-determining step (Figure S14). Plots of i_{cat}/i_p vs. [AcOH], in which i_p is the cathodic peak current in the absence of acid, confirm the second-order dependence on acid concentration (Figure S14).[7b] Additionally, varying $[\mathbf{1}](BF_4)_2$ concentrations at a fixed [AcOH] confirms a first-order dependence on the catalyst concentration (Figure S15). The overall rate of the reaction is, therefore, second order with respect to acid concentration and first order with respect to the concentration of Co-complex $[\mathbf{1}](BF_4)_2$. Control experiments with acetic acid in the absence of $[\mathbf{1}](BF_4)_2$ show no significant current in the potential window (Figure S16).

Initial robustness tests of the catalyst were carried out through controlled bulk electrolysis experiments using a mercury electrode, which showed that the complex is not stable for longer times (2 h) at an applied potential of −1.9 V. We also compared the charge consumed in the presence and absence of $[\mathbf{1}](BF_4)_2$ and noted a higher consumption of charge (Coulomb) when acetic acid (10 and 50 equivalents with respect to catalyst) was electrolyzed in the presence of $[\mathbf{1}](BF_4)_2$. The electrolysis experiments were performed for 30 minutes and the charge was 252 and 333 miliCoulomb (mC) in presence of 10 and 50 equivalent acetic acid, while without catalyst the charges were 155 and 230 mC, respectively (Figures S17–S18). The catalytic TON for $[\mathbf{1}](BF_4)_2$ calculated from this initial bulk electrolysis experiment amounts to 0.25, clearly showing that $[\mathbf{1}](BF_4)_2$ is not stable under experimental conditions using a Hg electrode. The dimethyl-substituted complex $[\mathbf{4}](BF_4)_2$ was also tested in presence of 50 equiv of AcOH. In this case, charge consumption in the presence and absence of the cobalt complex is very similar (Figure S18). This once more points out the importance of the acidic methylene unit in the ligand backbone for the reduction chemistry of $[\mathbf{1}](BF_4)$. Ongoing bulk chronoamperometric experiments using a rotating glassy carbon electrode in combination with in-line H_2-detection via GC target a more detailed picture on the durability of $[\mathbf{1}](BF_4)_2$ during electrocatalysis and aim to optimize its overall performance.

Mechanistic investigation

A number of reaction pathways for the electrocatalytic HER by $[\mathbf{1}](BF_4)_2$ have been examined by means of DFT calculations (for details see the Supporting Information). Based on the potential at which electrocatalysis takes place and the electrochemical properties of the Co-complexes discussed here, we considered that cobalt-centered reduction of $[\mathbf{1}]^{2+}$ is the initial step in the mechanism for H_2 evolution (Scheme 4). Next, complex **A**, formed upon 1-electron reduction of $[\mathbf{1}]^{2+}$, could undergo a 2-electron oxidation upon reaction with a proton to give rise to an intermediate Co^{III}–H complex, $[HCo^{III}(HBMIM^{Ph_2})_2]^{2+}$ (**B**).

The generation of H_2 from **B** could then proceed in two ways: i) complex **B** undergoes an electrochemical reduction to form an Co^{II}–H intermediate, $[HCo^{II}(HBMIM^{Ph_2})_2]^{+}$ (**C**), and the Co^{II}–H bond subsequently combines with one of the methylene protons of a $HBMIM^{Ph_2}$ ligand to form H_2 and $[\mathbf{2}]^{+}$ (formal heterolytic cleavage of the Co^{II}–H bond; pathway 1), or (ii) the Co^{III}–H bond and one of the methylene protons complex **B** combine through homolytic cleavage of the cobalt hydride bond to form H_2 and complex $[\mathbf{3}]^{2+}$, followed by electrochemical reduction of $[\mathbf{3}]^{2+}$ to form complex $[\mathbf{2}]^{+}$ (pathway 2). In the final step, complex $[\mathbf{2}]^{+}$ would be protonated to regenerate starting complex $[\mathbf{1}]^{2+}$. In the overall reaction, two protons and two electrons ($2H^{+} + 2e^{-}$) are then involved for the generation of H_2.

Several other possible pathways without involvement of the ligand C–H bond have been ruled out based on the experimental rate equation for the HER by $[\mathbf{1}](BF_4)_2$ and bulk electrolysis experiments of complex $[\mathbf{4}](BF_4)_2$. The overall rate of the electrocatalysis by $[\mathbf{1}](BF_4)_2$ in the presence of acid is first order with respect to catalyst, which indicates that the reaction goes through a mono-metallic pathway and discards bimolecular pathways such as the bimetallic homolytic cleavage of Co^{III}–H or Co^{II}–H complexes to generate Co^{II} and Co^{I} complexes, re-

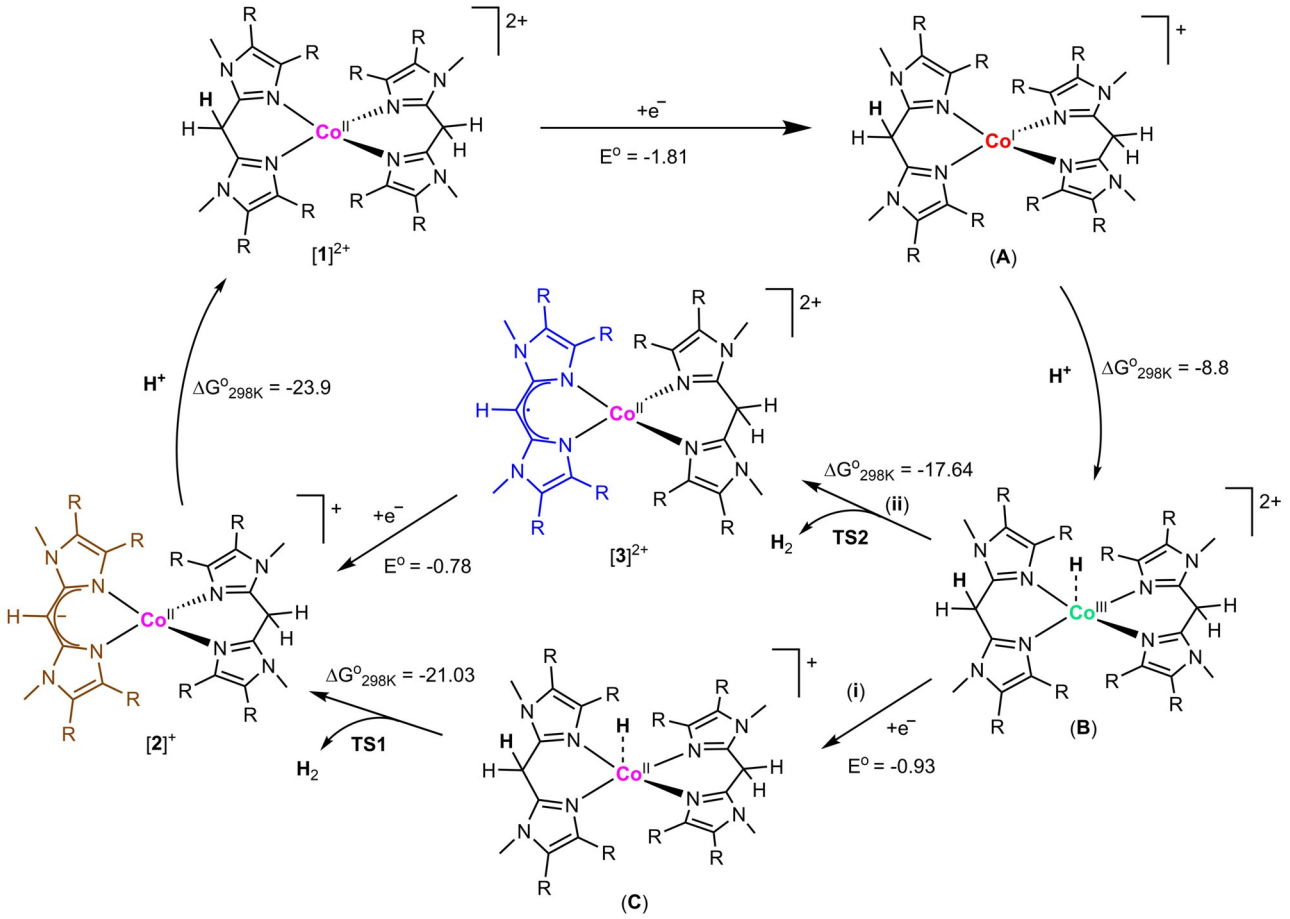

Scheme 4. Proposed mechanistic pathways of H^+ reduction by $[\mathbf{1}]^{2+}$ derived from a combination of experimental and theoretical (BP86) results, including calculated reduction potentials (E° in V vs. Fc/Fc^+) and free energy changes (ΔG^0_{298K} in kcal mol^{-1}) (R = Ph).

spectively, along with dihydrogen. Complex $[\mathbf{4}](BF_4)_2$ does not show any activity in bulk electrolysis experiments, which rules out the possibility of heterolytic cleavage of Co^{III}–H or Co^{II}–H species in the presence of the external proton source (acetic acid).

At the start of our DFT study we have optimized the geometries of the isolated complexes ($[\mathbf{1}]^{2+}$, $[\mathbf{2}]^+$ and $[\mathbf{3}]^{2+}$), proposed intermediates (**A**, **B** and **C**), and the possible transition states (**TS1** and **TS2**) to understand the full catalytic cycle for electrocatalytic hydrogen production using $[\mathbf{1}](BF_4)_2$. The DFT calculated spin density plot for $[\mathbf{1}]^{2+}$ supports the high spin configuration of the Co^{II} center. The 1-electron reduced intermediate **A** shows a Mulliken spin value of 1.9 localized on the Co center (Figure S20), suggesting that the first reduction indeed takes place at the cobalt(II) center and that **A** is a Co^{I} species. Upon reduction of $[\mathbf{1}]^{2+}$, a structural change from distorted tetrahedral for Co^{II} to distorted trigonal bipyramidal for Co^{I} is induced (Figure S21), which provides space for a fifth ligand to bind to cobalt. The calculated reduction potential for the $Co^{II/I}$ couple is -1.81 V_{Fc/Fc^+}, which is very close to the experimentally observed reduction potential ($E_p = -1.96$ V_{Fc/Fc^+}). The formation of intermediate **B** from intermediate **A** via oxidative addition of a proton to the Co^{I} center was computed to be favorable by 8.8 kcal mol^{-1}. To compute this value, the literature value of -266.5 kcal mol^{-1} was used for the free energy of a proton in CH_3CN solvent (vide infra).[35] Intermediate **B** was optimized in two spin states *viz.* intermediate spin Co^{III} with $S = 1$ and low spin Co^{III} with $S = 0$. The former spin state is energetically favored by 12.9 kcal mol^{-1}. The optimized geometry of **B** indicates that one of the six-membered Co(NCCCN) chelate rings adopts a boat-like configuration, which preorganizes the methylene C1–H2 bond in the corresponding $HBMIM^{Ph_2}$ ligand and the Co1–H3 bond with respect to each other (Figure 8a). The computed Co1–H3 distance in **B** is 1.456 Å, which is comparable with reported Co^{III}–H distances.[23]

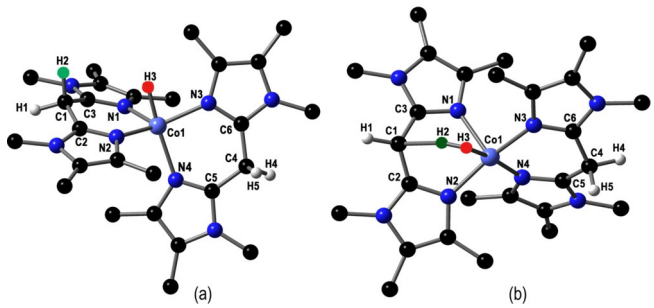

Figure 8. Optimized geometries of (a) complex B and (b) TS1[d] (phenyl groups are omitted for clarity).

Next, dihydrogen evolution may proceed via either pathway 1 or 2, as indicated above. The first step in pathway 1 is the reduction of the intermediate Co^{III}–H complex (**B**) to form a Co^{II}–H intermediate (**C**). The calculated reduction potential for this transformation is $-0.93\ V_{Fc/Fc^+}$, which is energetically favorable with respect to the experimentally applied potential. Intermediate **C** was also optimized in two spin states, *viz.* a low spin Co^{II} ($S=1/2$) and a high spin Co^{II} ($S=3/2$) state. The low spin Co^{II} state is energetically more favorable than the high spin state by 16.3 kcal mol^{-1}, likely a consequence of the strong-field hydride ligand. Subsequent generation of dihydrogen via heterolytic cleavage of the Co^{II}–H bond is energetically favored by 21.03 kcal mol^{-1}. The transition state (**TS1**) for this transformation was also optimized in two different spin states, *viz.* a doublet (**TS1 d**, Figure 8b) and quartet (**TS1 q**) state. The doublet state is 3.8 kcal mol^{-1} lower in energy than the quartet state and the activation barrier towards **TS1 d** is 20.8 kcal mol^{-1}. Comparison of the metrical parameters of these two transition states reveals that **TS1 d** has the more product-like geometry (Table S2). For example, the d_{H-H} and the sum of the angles around the central carbon atom (∡C3-C1-C2 + ∡H1-C1-C3 + ∡H1-C1-C2) in the participating $HBMIM^{Ph_2}$ ligand in **TS1 d** are 0.863 Å and 353°, respectively, while these values are 1.115 Å and 346° in **TS1 q**. The intraligand bond distances and angles in the participating $HBMIM^{Ph_2}$ ligand are different from those in the spectator ligand: d_{C1-C2} and d_{C1-C3} distances in the participating ligand are contracted by ≈0.05 Å compared to the spectator ligand (d_{C4-C5} and d_{C4-C6}; Table S2).

The first step in pathway 2 is the generation of dihydrogen from intermediate **B** via homolytic cleavage of the C1–H2 bond and Co1–H3 bond, which is energetically favored by 17.6 kcal mol^{-1} and has an activation energy towards **TS2** of 25.0 kcal mol^{-1}. The optimized structure of **TS2** is shown in Figure S22. The resulting complex $[\mathbf{3}]^{2+}$ undergoes electrochemical reduction to form complex $[\mathbf{2}]^{+}$ in the subsequent step. The calculated reduction potential for this step is $-0.78\ V_{Fc/Fc^+}$, which is comparable with the experimentally observed first oxidation potential of $[\mathbf{2}]^{+}$ ($-0.66\ V_{Fc/Fc^+}$). The final step for both pathways is the regeneration of $[\mathbf{1}]^{2+}$ from $[\mathbf{2}]^{+}$ upon acceptance of a proton from solution, which is energetically favorable by 23.9 kcal mol^{-1}.

An alternative pathway that was also considered proceeds via H-atom transfer from the ligand (homolytic cleavage of C–H bond) to Co^{I} in molecule **A** to generate a Co^{II}–H intermediate, $[Co^{II}H(HBMIM^{Ph_2})(BMIM^{Ph_2\bullet})]^{+}$ (**B′**) with a radical ligand (Figure S22). The overall H-atom transfer to form this Co^{II}–H intermediate (**A**→**B′**) is energetically favorable by 14.5 kcal mol^{-1}. The energy barrier (**TS′**) for this transformation is 27.5 kcal mol^{-1} (SI, Figure S22A). The optimized geometry of **TS′** is shown in Figure 9.

The next step along this reaction trajectory is the reduction of the radical ligand in **B′** to form Co^{II}–H species **C′** with an anionic ligand. The calculated reduction potential for this step is $-2.66\ V_{Fc/Fc^+}$, which is energetically unfavorable with respect to the experimentally applied potential. The subsequent protonation of the anionic ligand in **C′** to generate complex **C** is energetically favorable ($\Delta G^0_{298K} = -34.07$ kcal mol^{-1}). This reaction trajectory via H-atom transfer is also shown in Figure 10.

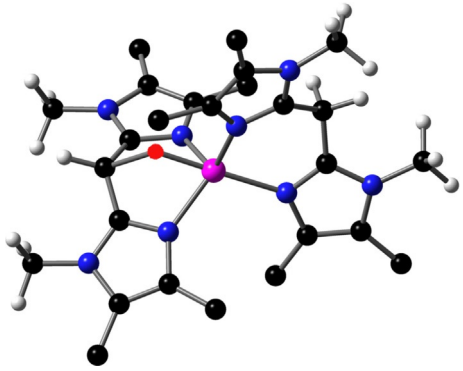

Figure 9. Optimized geometry of TS′ (phenyl groups are omitted for clarity).

While these DFT studies are not conclusive for the overall reaction pathway of the HER reaction catalyzed by $[\mathbf{1}](BF_4)_2$, they do indicate the common involvement in the three pathways discussed above of a C–H bond of the $HBMIM^{Ph_2}$ ligand backbone in the H–H bond forming step. Dihydrogen formation in these pathways seems to proceed via a formal heterolytic cleavage of a Co^{II}–H bond in intermediate **C** and through transition state **TS1 d**. On the other hand, the calculations are not conclusive on each individual reaction step that precedes dihydrogen formation, in particular on steps related to the formation of intermediates **B**/**B′** and **C**/**C′**. A reason for this may be that our calculations may overestimate the difference in reduction potential between species of different charge. In addition, one could scrutinize the free energy that was used for the solvated proton with respect to the conditions of catalysis.

Lastly, another pathway proceeding via direct elimination of H_2 from $Co^{II}H$ intermediate **B′**, $[Co^{II}H(HBMIM^{Ph_2})(BMIM^{Ph_2\bullet})]$ via participation of a methylene proton of the other, neutral ligand was found to be energetically unfavorable ($\Delta G^0_{298K} = +7.7$ kcal mol^{-1}), with an activation barrier of 49.7 kcal mol^{-1} (Figure S23). While the alternative, mononuclear pathways seems unfavorable with respect to the pathway depicted in

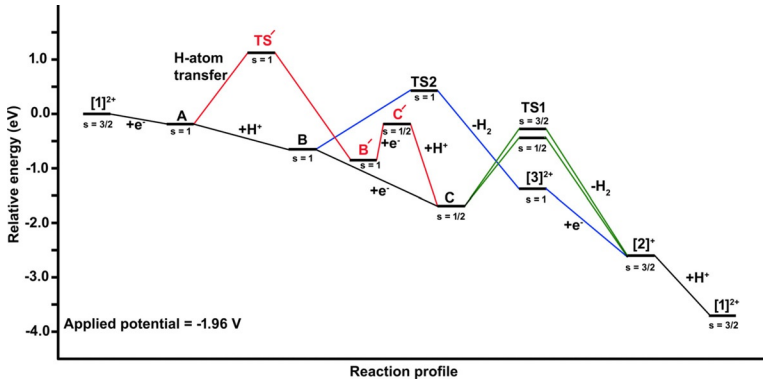

Figure 10. Overall reaction energy diagram for catalytic proton reduction by $[\mathbf{1}](BF_4)_2$ derived from DFT calculations. Spin state (*s*) of isolated complexes, proposed intermediates and TSs are mentioned.

Scheme 4, we can at the moment not rule out a rapid, non-rate limiting bimetallic pathway involving two complexes.

Conclusions

We have reported on the tetrahedral cobalt complex [**1**]$(BF_4)_2$, derived from the bidentate imidazole ligand $HBMIM^{Ph_2}$, that can act as an electrocatalyst for the HER reaction using a weak proton source. Isolation and characterization of the corresponding 1-electron reduced complex [**2**](BF_4) have established that upon reduction of [**1**]$(BF_4)_2$ a methylene C–H proton from the ligand backbone expels an H-atom, presumably as dihydrogen. Formally deprotonated complex [**2**](BF_4) regenerates the starting complex [**1**]$(BF_4)_2$ in the presence of a proton source. Subsequent experiments have shown that [**1**]$(BF_4)_2$ is able to act as a catalyst in the electrocatalytic HER reaction. DFT calculations in combination with electrochemical studies suggest that the coordinated $HBMIM^{Ph_2}$ ligand acts as a reversible proton-shuttle in the HER by [**1**]$(BF_4)_2$. H–H bond formation in the proposed mechanism takes place in an intramolecular fashion through transition state **TS1 d**, in which a Co–H bond and a methylene C–H bond of the ligand backbone approach each other. While our DFT calculations do suggest the involvement of a ligand C–H bond in hydrogen formation, these calculations are less conclusive on the reaction steps preceding the actual H–H bond formation step, that is, the steps that are involved in the formal reduction and protonation steps preceding H_2 formation.

Notably, participation of pendant proton donors (or proton shuttles) like N–H or COOH moieties in HER catalysis is well documented, as pointed out in the introduction. The use of a C–H bond in combination with a metal hydride to form dihydrogen in an electrocatalytic manner has to the best of our knowledge not been noted before. On the other hand, reversible splitting/generation of dihydrogen via participation of a ligand backbone and a metal hydride has been noted for transition metal-pincer complexes. In these pincer complexes, the ligands undergo aromatization/dearomatization via deprotonation of a methylene unit and these complexes are commonly used in catalytic hydrogen transfer and hydrofunctionalization reactions.[4,36–39]

Accordingly, our observations on the electrochemical behavior of complex [**1**]$(BF_4)_2$ and on its use in electrocatalytic HER may be of relevance to the design of responsive ligands[40] and their use in HER and other reactions. Efforts towards a further development of ligands related to $HBMIM^{Ph_2}$ and their use in HER catalysis are ongoing in our laboratories and, amongst other, are focused on improving TON and overpotential values in HER catalysis and on a further mechanistic understanding.

Experimental Section

Experimental details, synthesis and characterization of the relevant complexes, and DFT calculation results are available in the Supporting Information.

CCDC 1877825, 1877826, and 1877827 contain the supplementary crystallographic data for this paper. These data are provided free of charge by The Cambridge Crystallographic Data Centre.

Acknowledgements

P.G. acknowledges the European Union for Marie Curie Post-doctoral Fellowship support (grant number-657765). This work was sponsored by NWO Exacte en Natuurwetenschappen (Physical Sciences) for the use of supercomputer facilities, with financial support from the Nederlandse Organisatie voor Wetenschappelijk Onderzoek (Netherlands Organization for Scientific Research, NWO). The X-ray diffractometer has been financed by NWO. Chronoamperometry was carried at the Inorganic Chemistry & Catalysis group at Utrecht University; Marisol Tapia Rosales is thanked for practical assistance. The authors are thankful to Dr. Dennis Hetterscheid (Leiden University) for fruitful discussions.

Conflict of interest

The authors declare no conflict of interest.

Keywords: cobalt complex · DFT · diimine ligand · electrocatalysis · proton reduction

[1] J. A. Turner, *Science* **2004**, *305*, 972–974.
[2] N. S. Lewis, D. G. Nocera, *Proc. Natl. Acad. Sci. USA* **2006**, *103*, 15729–15735.
[3] K. J. Lee, N. Elgrishi, B. Kandemir, J. L. Dempsey, *Nat. Rev. Chem.* **2017**, *1*, 1–14.
[4] L. V. A. Hale, N. K. Szymczak, *ACS Catal.* **2018**, *8*, 6446–6461.
[5] N. Queyriaux, R. T. Jane, J. Massin, V. Artero, M. Chavarot-Kerlidou, *Coord. Chem. Rev.* **2015**, *304–305*, 3–19.
[6] C. C. L. McCrory, C. Uyeda, J. C. Peters, *J. Am. Chem. Soc.* **2012**, *134*, 3164–3170.
[7] a) X. Hu, B. M. Cossairt, B. S. Brunschwig, N. S. Lewis, J. C. Peters, *Chem. Commun.* **2005**, 4723–4725; b) X. Hu, B. S. Brunschwig, J. C. Peters, *J. Am. Chem. Soc.* **2007**, *129*, 8988–8998.
[8] M. L. Helm, M. P. Stewart, R. M. Bullock, M. R. DuBois, D. L. DuBois, *Science* **2011**, *333*, 863–866.
[9] S. Wiese, U. J. Kilgore, D. L. DuBois, R. M. Bullock, *ACS Catal.* **2012**, *2*, 720–727.
[10] R. M. Bullock, A. M. Appel, M. L. Helm, *Chem. Commun.* **2014**, *50*, 3125–3143.
[11] W. R. McNamara, Z. Han, C.-J. Yin, W. W. Brennessel, P. L. Holland, R. Eisenberg, *Proc. Natl. Acad. Sci. USA* **2012**, *109*, 15594–15599.
[12] W. R. McNamara, Z. Han, P. J. Alperin, W. W. Brenessel, P. L. Holland, R. Eisenberg, *J. Am. Chem. Soc.* **2011**, *133*, 15368–15371.
[13] D. K. Bediako, B. H. Solis, D. K. Dogutan, M. M. Roubelakis, A. G. Maher, C. H. Lee, M. B. Chambers, S. Hammes-Schiffer, D. G. Nocera, *Proc. Natl. Acad. Sci. USA* **2014**, *111*, 15001–15006.
[14] D. J. Graham, D. G. Nocera, *Organometallics* **2014**, *33*, 4994–5001.
[15] T. J. Sherbow, J. C. Fettinger, L. A. Berben, *Inorg. Chem.* **2017**, *56*, 8651–8660.
[16] E. J. Thompson, L. A. Berben, *Angew. Chem. Int. Ed.* **2015**, *54*, 11642–11646; *Angew. Chem.* **2015**, *127*, 11808–11812.
[17] A. Z. Haddad, B. D. Garabato, P. M. Kozlowski, R. M. Buchanan, C. A. Grapperhaus, *J. Am. Chem. Soc.* **2016**, *138*, 7844–7847.
[18] A. Z. Haddad, D. Kumar, K. O. Sampson, A. M. Matzner, M. S. Mashuta, C. Grapperhaus, *J. Am. Chem. Soc.* **2015**, *137*, 9238–9241.

[19] C. Elleouet, F. Y. Pétillon, P. Schollhammer, in *Non-Noble Metal Catalysis: Molecular Approaches and Reactions*. (Eds.: R. J. M. Klein Gebbink, M. Moret) Wiley-VCH Verlag GmbH & Co. KGaA, **2019**, Ch. 18, pp. 489 – 527.
[20] J. R. McKone, S. C. Marinescu, B. S. Brunschwig, J. R. Winkler, H. B. Gray, *Chem. Sci.* **2014**, *5*, 865 – 878.
[21] B. H. Solis, S. Hammes-Schiffer, *J. Am. Chem. Soc.* **2012**, *134*, 15253 – 15256.
[22] C. S. Letko, J. A. Panetier, M. Head-Gordon, T. D. Tilley, *J. Am. Chem. Soc.* **2014**, *136*, 9364 – 9376.
[23] J. A. Panetier, C. S. Letko, T. D. Tilley, M. Head-Gordon, *J. Chem. Theory Comput.* **2016**, *12*, 223 – 230.
[24] D. Moonshiram, C. Gimbert-Suriñach, A. Guda, A. Picon, C. S. Lehmann, X. Zhang, G. Doumy, A. M. March, J. Benet-Buchholz, A. Soldatov, A. Llobet, S. H. Southworth, *J. Am. Chem. Soc.* **2016**, *138*, 10586 – 10596.
[25] S. Fukuzumi, Y. Yamada, T. Suenobu, K. Ohkubo, H. Kotani, *Energy Environ. Sci.* **2011**, *4*, 2754 – 2766.
[26] B. H. Solis, A. G. Maher, D. K. Dogutan, D. G. Nocera, S. Hammes-Schiffer, *Proc. Natl. Acad. Sci. USA* **2016**, *113*, 485 – 492.
[27] M. H. V. Huynh, T. J. Meyer, *Chem. Rev.* **2007**, *107*, 5004 – 5064.
[28] J. J. Warren, T. A. Tronic, J. M. Mayer, *Chem. Rev.* **2010**, *110*, 6961 – 7001.
[29] C. Costentin, M. Robert, J.-M. Savéant, *Acc. Chem. Res.* **2010**, *43*, 1019 – 1029.
[30] P. Ghosh, R. Naastepad, C. F. Riemersma, M. Lutz, M.-E. Moret, R. J. M. Klein Gebbink, *Chem. Eur. J.* **2017**, *23*, 10732 – 10737.
[31] M. M. Khusniyarov, E. Bill, T. Weyhermüller, E. Bothe, K. Wieghardt, *Angew. Chem. Int. Ed.* **2011**, *50*, 1652 – 1655; *Angew. Chem.* **2011**, *123*, 1690 – 1693.
[32] M. J. Frisch, et al., *Gaussian 09*, Gaussian, Inc., Wallingford, CT, USA, **2013**.
[33] V. Fourmond, P. A. Jacques, M. Fontecave, V. Artero, *Inorg. Chem.* **2010**, *49*, 10338 – 10347.
[34] A. M. Appel, M. L. Helm, *ACS Catal.* **2014**, *4*, 630 – 633.
[35] C. P. Kelly, C. J. Cramer, D. G. Truhlar, *J. Phys. Chem. B* **2007**, *111*, 408 – 422.
[36] C. Gunanathan, D. Milstein, *Acc. Chem. Res.* **2011**, *44*, 588 – 602.
[37] C. Gunanathan, D. Milstein, *Chem. Rev.* **2014**, *114*, 12024 – 12087.
[38] T. Zell, D. Milstein, *Acc. Chem. Res.* **2015**, *48*, 1979 – 1994.
[39] A. Lukas, M. Fritz, S. Schneider, *Chem. Rev.* **2019**, *119*, 2681 – 2751.
[40] A. Chirila, B. G. Das, P. F. Kuijpers, V. Sinha, B. de Bruin, in *Non-Noble Metal Catalysis: Molecular Approaches and Reactions*. (Eds.: R. J. M. Klein Gebbink, M.-E. Moret) Wiley-VCH Verlag GmbH & Co. KGaA, **2019**, Ch. 1, pp. 1 – 31.

Manuscript received: December 20, 2019
Revised manuscript received: April 19, 2020
Accepted manuscript online: April 30, 2020
Version of record online: September 4, 2020